03

Saturn hexagon as a form of internal Stokes waves

© E.L. Amromin

Federal Way WA 98003, USA
e-mail: amromin@aol.com

Received May 8, 2024
Revised July 6, 2024
Accepted July 7, 2024

Observations show a hexagon of the very regular shapes with equal corners of practically 120 degrees on the Saturn surface. There are already several theories aimed to explain appearance of these corners. On the other hand, such corners are inherent to Stokes waves and these waves can have the various nature. In this study a simplified 2D problem on inner Stokes waves within a circle with two incompressible fluids of slightly diverse densities and a vortex with the center coinciding with the center of this circle originates is considered; the steady flows exist inside and outside the inner wave surface separating two fluids. Its shape is determined via solving the corresponding nonlinear free-surface problems. Numerical solutions for various ratios of fluid densities and circle radius to hexagon side size are compared with the observed hexagon.

Keywords: Velocity potential, inner Stokes waves, jump of density, iterations in the numerical method.

DOI: 10.61011/TP.2024.10.59355.163-24

Introduction

A regular hexagon with well-defined angles of 120° is seen in various photographic images of the surface of Saturn. A simplified diagram of an image of this kind is shown in Fig. 1. The corresponding atmospheric flow has been examined multiple times in numerical studies, and various hypotheses regarding its origin have been proposed. Notably, polygonal figures emerge in various flows. They may exist between rotating disks [1,2] and around rotating multi-bladed devices [3]. These figures are not induced by turbulence, although this formation mechanism has been suggested in certain studies. It was also noted [4] that „a stable hexagonal structure can emerge . . . when dynamic instabilities in the zonal jet nonlinearly equilibrate."

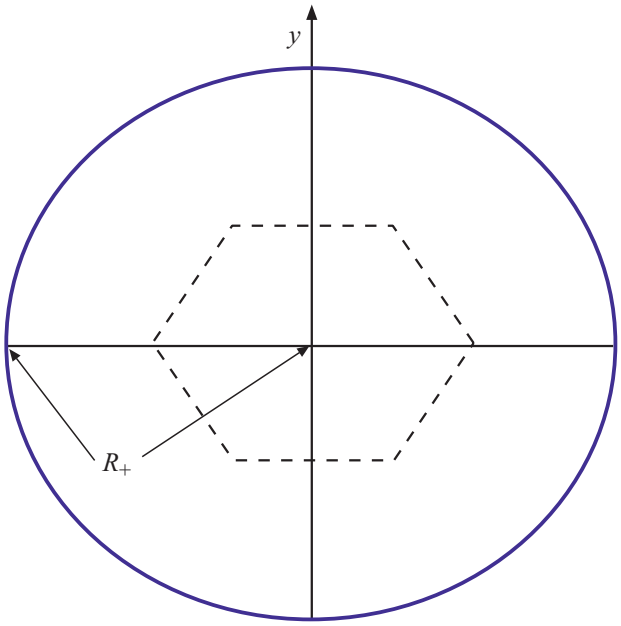

Figure 1. Sketch of a hexagon inside a circle. The sides of the hexagon are curved slightly, but the angles are 120°.

At the same time, angles of 120° are characteristic of various steady Stokes waves. Gravity-induced Stokes waves in two-dimensional flows have been studied since [5]. A nearly complete review of research in this field may be found in [6]. Stokes waves may also be caused by centrifugal forces in axisymmetric flows [7]. In addition, according to [8], inner Stokes waves caused by a density jump inside the flows are possible. This is the wave type examined below.

1. Inner Stokes waves inside a circle

Let us consider a simplified scenario with two fluids of different densities inside a circle with radius R_+. According to [9], two vortices are present inside the hexagon above Saturn, but only one of them produces a significant contribution to the velocities along the hexagon's contour. Let us assume that the inner fluid with density ρ_- occupies the core of a vortex with maximum radius R_- equal to the side length of the hexagon; introducing polar coordinates with radius r normalized to R_-, one obtains $R_- = 1.0$. Given the scale of the examined planetary flow, it must be turbulent. Then, as was demonstrated in [10], the asymptotic solution of the Reynolds equations [11] may be used to approximate the circumferential velocity inside the vortex core:

$$U_{\theta-} = r[1 - \ln(r)]. \quad (1)$$

Here, $U_{\theta-}$ is normalized to ωR_-, where ω is the rotation frequency. This formula was obtained under the assumption of an insignificant dependence of turbulent stresses on

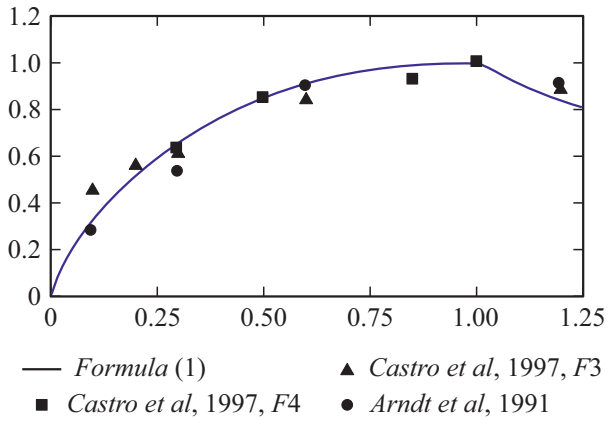

Figure 2. Comparison of formula (1) with distributions of the normalized measured azimuthal velocity along the vortex radius.

coordinates. Figure 2 demonstrates that formula (1) agrees closely with the experimental data reported in [12,13].

The outer fluid has density $\rho_+ = \varepsilon\rho_-$ and is also rotating. Boundary S between the two fluids of different densities is impermeable, and the pressure should be the same on both sides of S. Therefore, S will be a free surface. The entire flow is not vortex-free, but flow disturbances caused by the dependence of S on azimuth θ may be specified using the velocity potentials. One of the potentials is defined inside the hexagon. It satisfies the Laplace equation and boundary condition

$$\frac{\partial\Phi_-}{\partial N} + r[1 - \ln(r)]N_r = 0. \tag{2}$$

Here, N_r is the radial component of the normal to S. Another velocity potential outside S needs to be introduced. This potential must satisfy condition

$$\frac{\partial\Phi_+}{\partial N} + r[1 - \ln(r)]N_r = 0 \tag{3}$$

on S and at $r = R_+$. However, it was noted in [8] that when inner Stokes waves with crest angles of 120° are considered, it is necessary to introduce certain initially unknown circulation (or certain vortices) in the outer flow around the angles of 240°. Therefore, in addition to the potential of monopoles with intensity Q_+, Φ_+ includes the potential of vortices of initially unknown intensity γ that may be determined using the asymptotics

$$\lim_{s\to 0} U_+ = \sqrt{s}, \tag{4}$$

which was derived in [8] with the use of conformal mappings. Here, abscissa s is measured from the crest (according to [9], high-vorticity zones should actually be located near each vertex of the hexagon). The solution of Eqs. (2) and (3) is simplified by the fact that the velocity distributions over all parts of the hexagon match each other.

The condition of continuity of pressure in passing through S needs to be used to determine S. It may be written as

$$U_-^2 = \varepsilon U_+^2 \tag{5}$$

along the entire S. The necessity of fulfilling Eq. (5) leads to the deviation of sides of the hexagon from straight segments between the vertices. The procedure for determining these deviations $h(s)$ is similar to the procedures discussed in [8] in the context of other problems of free-boundary potential theory. Such problems are nonlinear, and iterations are needed to solve them. In each iteration, quasi-linearization of Eqs. (2) and (3) with the use of perturbations of both potentials with small intensities q_- and q_+ yields equations

$$q_+ = 2d(hU_+)/ds, \quad q_- = -2\frac{d(hU_-)}{ds}. \tag{6}$$

In addition, condition

$$U_-\int_0^s q_+ds + U_+\int_0^s q_-ds = 0 \tag{7}$$

is satisfied along S.

Since the velocity perturbations are about Cauchy integrals of intensity q_- or q_+, quasi-linearization of Eq. (5) leads to the equation

$$\frac{1}{\pi}\int_0^1 \frac{\mu q_+ - q_-}{s-\tau}d\tau + 2h[(\mu-1)(1-\ln|r|)]2U_+d\mu = 2(U_- - \mu U_+) \tag{8}$$

along the top horizontal side of the hexagon. Here, $\mu = \sqrt{\varepsilon}$. Equation (8) may be simplified further by inverting the Cauchy integrals, and

$$\mu q_+ - q_- + \frac{F\{s\}}{\pi}\int_0^1 \left[\frac{(\mu-1)(1-\ln|r|)}{U_-}\left(\int_0^\tau q_-d\xi\right) - 2U_+d\mu\right]\frac{d\tau}{(s-\tau)F\{\tau\}} = 2\frac{F\{s\}}{\pi}\int_0^1 \frac{(U_- - \mu U_+)}{(s-\tau)F\{\tau\}}d\tau \tag{9}$$

Here, $F\{s\} = \sqrt{s(1-s)}$. However, as was noted in [14], this inversion is possible only on the additional condition that

$$\int_0^1 \left[\frac{(1-\ln|r|)}{U_-}(1-\mu)\left(\int_0^\tau q_-d\xi\right) + 2(U_+d\mu)\right] \times \frac{d\tau}{F\{\tau\}} + 2\int_0^1 \frac{(U_- - \mu U_+)}{F\{\tau\}}d\tau = 0, \tag{10}$$

and the necessity of fulfilling Eq. (10) is related to the definition of variation $d\mu$ of parameter μ in the entire problem. Having solved Eqs. (7)–(10), one may find function $h(s)$ by integrating one of the equations from (6) and correct S. This correction of S may be interpreted as motion against the gradient in the auxiliary space

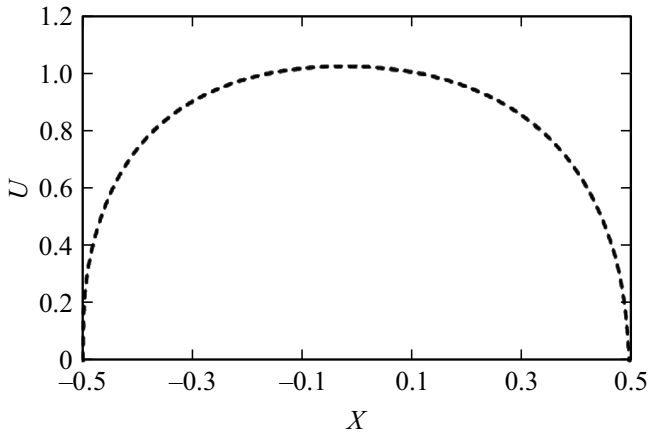

Figure 3. Example distribution of U_+ along S.

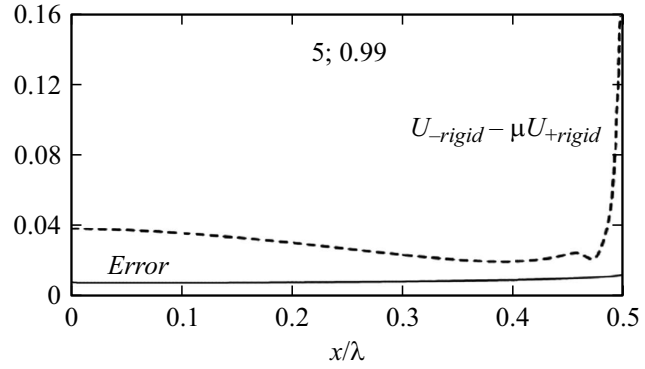

Figure 4. Illustration of the algorithm convergence. The solid line designated as „error" corresponds to the absolute value of difference $U_- - \mu U_+$ after seven iterations.

of variables defining surface S. Although an analytical description of this surface may exist, the general approach is to correct it stepwise using M points distributed over the examined part of S. Let us denote the coordinates of these points as

$$x_m^{k+1} = x_m^k + \alpha h_m^k N_{xm}^k, \quad y_m^{k+1} = y_m^k + \alpha h_m^k N_{ym}^k, \qquad (11)$$

where superscripts and subscripts indicate iteration and point numbers, respectively. The definition of $h(s)$ allows for calculation of the components of the h_m^k anti-gradient on S, but the strong nonlinearity of the problem makes it necessary to move in small steps along this anti-gradient. Therefore, positive factor $\alpha \ll 1$ is introduced into Eq. (11). An example calculated velocity distribution is shown in Fig. 3. The X coordinate is measured from the center of the hexagon, and the x axis is perpendicular to the y axis shown in Fig. 1.

The iteration convergence is illustrated in Fig. 4 for $R_+ = 5$ and $\varepsilon = 0.99$. A regular hexagon was chosen to be used as an initial approximation to unknown surface S. The distributions of $U_{+\text{rigid}}$ and $U_{-\text{rigid}}$ along it were inserted into Eq. (5), and the corresponding difference $U_- - \mu U_+$ is compared in Fig. 4 to a similar difference along S obtained after seven iterations.

2. Qualitative comparison with observations

The observed [15] and calculated hexagon shapes are compared in Fig. 5. Their sides are very similar.

The maximum deviation A of the hexagon side from a straight segment between its two vertices is close to the height of a classical Stokes wave, while the segment length is similar to wavelength λ. These similarities allow us to make certain comparisons. The A/λ ratio for two-dimensional gravity Stokes waves decreases from 0.142 for a flow of infinite depth to 0.098 for a flow of minimum depth (defined according to [16] as the minimum depth at which these steady waves are supported). Keeping in mind the analogy between the above-mentioned depth and the distance between the hexagon and the surrounding circle, one may spot the same trend in Fig. 6.

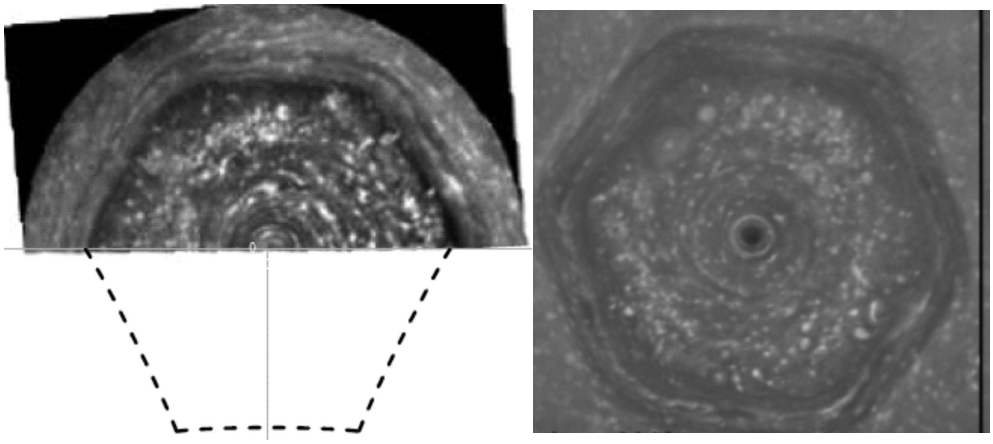

Figure 5. Comparison of the calculated hexagon shape (dotted curve at the bottom in the left panel) and the photographic image of the hexagon above Saturn.

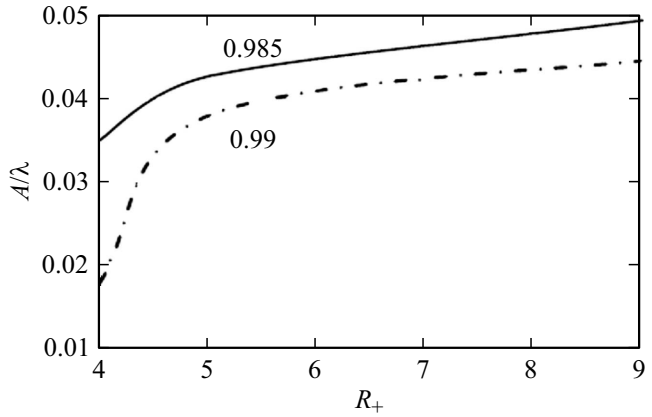

Figure 6. Influence of the circle radius on the wave steepness. The numbers next to the curves indicate the corresponding density ratios.

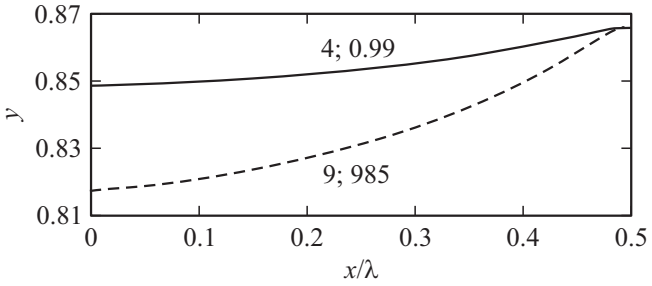

Figure 7. Shapes of hexagon sides for $\{R_+ = 4, \varepsilon = 0.99\}$ and $\{R_+ = 9,\ \varepsilon = 0.985\}$.

More detailed images of surface S (the surface of these inner waves) are shown in Fig. 7. At $x = \lambda/2$ dy/dx undergoes a jump from 0 to $-\tan(\pi/6)$. The shapes of shown S shown in Figs. 1 and 5 correspond to $\{R_+ = 4,\ \varepsilon = 0.99\}$. Notably, $R_+ = 4$ is close to the ratio between the diameter of Saturn and the observed [17] size of its hexagon.

The comparison presented in Fig. 5 is qualitative. However, it is sufficiently compelling to put forward a hypothesis that the hexagon is a type of inner Stokes waves. The results of laboratory experiments with certain polygonal structures in fluids (e.g., [3,18,19]) are less convincing. The examination of asymmetric potential disturbances of one fluid (similar to those discussed in [2], but caused by a moon) did not yield any polygonal figure.

In quantitative analysis, the considered flow should be three-dimensional, and gravity also needs to be taken into account. This might be feasible in the axisymmetric approach [20], but requires the substitution of an outer rigid circle with an inner rigid sphere and the use of certain data regarding the bottom of the flow. However, the method for solving the free surface problem will be quite similar (it will be a mere modification of the method of Ivanov).

Conclusion

The hexagon observed above Saturn has been studied by numerous research groups, but the concepts used in their work were not supported by sufficient evidence. Therefore, the application of an alternative approach is reasonable, and this hexagon was regarded in the present study as the surface of an inner Stokes wave forming between two fluids of different densities. The flow was assumed to be induced by an axisymmetric vortex, and deformations of the hexagon surface were characterized by vortex-free flow potentials. The discussed iterative procedure for solving the corresponding nonlinear problem was verified by comparison with solutions of other problems on Stokes waves with crest angles of 120°.

It can be said that the comparison of shapes of the calculated and observed hexagons revealed their close agreement, since the considered model inner-wave problem allowed us to reproduce the hexagonal structure, and the degree of deviation of the hexagon sides from straight segments is difficult to estimate from the available photographic images.

Conflict of interest

The author declares that he has no conflict of interest.

References

[1] S.D. Abrahamson, J.K. Eaton, D.J. Koga. Phys. Fluids, **1**, 241 (1989).
[2] E.L. Amromin, S.I. Kovinskaya. J. Fluids and Structures, **34**, 84 (2012).
[3] T.R.N. Jansson, M.P. Haspang, K.H. Jensen, P. Hersen, T. Bohr. Phys. Rev. Lett., **96**, 174502 (2006).
[4] R. Morales-Juberías, K.M. Sayanagi, T.E. Dowling, A.P. Ingersoll. Icarus, **211**, 1284 (2011).
[5] J.H. Michel. Phil. Magazine, **36** (5), 430 (1893).
[6] X. Zhong, S.J. Liao. Fluid Mechanics, **843**, 653 (2018).
[7] E.L. Amromin. Fluid Dyn., **31** (6), 886 (1996).
[8] E.L. Amromin. Tech. Phys., **93** (1), 48 (2023). DOI: 10.21883/TP.2023.01.55439.212-22
[9] M. Rostami, V. Zeitlin, A. Spiga. Icarus, **297**, 59 (2017).
[10] E.L. Amromin. Phys. Fluids, **19**, 118108 (2007).
[11] L.I. Sedov. *Mekhanika sploshnoi sredy* (Nauka, M., 1976), Vol. II (in Russian).
[12] R.E.A. Arndt, V.H. Arakeri, H. Higuchi. J. Fluid Mech., **229**, 269 (1991).
[13] E. Castro, A. Crespo, F. Manuel, D.H.J. Fruman. ASME J. Fluids Eng., **119**, 759 (1997).
[14] P.P. Zabreiko, A.I. Koshelev, M.A. Krasnosel'skii, C.G. Mikhlin, L.S. Rakovshchik, V.Ya. Stetsenko. *Integral'nye uravneniya* (Nauka, M., 1968) (in Russian).
[15] K. Baines, M. Flasar, N. Krupp, T. Stallard. *Saturn in the 21st Century* (Cambridge University Press, 2019)
[16] E.L. Amromin, A.N. Ivanov, D. Yu. Sadovnikov, Fluid Dyn., **29**, 540 (1994).
[17] S.K. Atreya, T.C. Owen, S.J. Bolton, T. Guillot. Int. Planetary Probe Workshop, IPPW-3, ESA SP-WPP263 (2006).

[18] R. Bergmann, L. Tophoj, T.A.M. Homan, P. Hersen, A. Andersen, T. Bohr. J. Fluid Mech., **679**, 415 (2011).
[19] A.C.B. Aguiar, P.L. Read, R.D. Wordsworth, T. Salter, Y.H. Yamazaki. Icarus, **206**, 755 (2010).
[20] R. Plougonven, V. Zeitlin. Phys. Fluids, **14**, 1259 (2002).

Translated by D.Safin